The Cryosphere Discuss., 9, 3959–3993, 2015
www.the-cryosphere-discuss.net/9/3959/2015/
doi:10.5194/tcd-9-3959-2015

The Cryosphere Discussions
Open Access

Long-term coastal-polynya dynamics in the Southern Weddell Sea from MODIS thermal-infrared imagery

S. Paul, S. Willmes, and G. Heinemann

Department of Environmental Meteorology, University of Trier, Trier, Germany

Received: 9 June 2015 – Accepted: 13 July 2015 – Published: 28 July 2015

Correspondence to: S. Paul (paul@uni-trier.de)

Published by Copernicus Publications on behalf of the European Geosciences Union.

Abstract

Based upon high-resolution thermal-infrared Moderate-Resolution Imaging Spectroradiometer (MODIS) satellite imagery in combination with ERA-Interim atmospheric reanalysis data, we derived long-term polynya parameters such as polynya area, thin-ice thickness distribution and ice-production rates from daily cloud-cover corrected thin-ice thickness composites. Our study is based on a thirteen year investigation period (2002–2014) for the austral winter (1 April to 30 September) in the Antarctic Southern Weddell Sea. The focus lies on coastal polynyas which are important hot spots for new-ice formation, bottom-water formation and heat/moisture release into the atmosphere. MODIS has the capability to resolve even very narrow coastal polynyas. Its major disadvantage is the sensor limitation due to cloud cover. We make use of a newly developed and adapted spatial feature reconstruction scheme to account for cloud-covered areas. We find the sea-ice areas in front of Ronne and Brunt Ice Shelf to be the most active with an annual average polynya area of 3018 ± 1298 and $3516 \pm 1420\,km^2$ as well as an accumulated volume ice production of 31 ± 13 and $31 \pm 12\,km^3$, respectively. For the remaining four regions, estimates amount to $421 \pm 294\,km^2$ and $4 \pm 3\,km^3$ (Antarctic Peninsula), $1148 \pm 432\,km^2$ and $12 \pm 5\,km^3$ (Iceberg A23A), $901 \pm 703\,km^2$ and $10 \pm 8\,km^3$ (Filchner Ice Shelf) as well as $499 \pm 277\,km^2$ and $5 \pm 2\,km^3$ (Coats Land). Our findings are discussed in comparison to recent studies based on coupled sea-ice/ocean models and passive-microwave satellite imagery, each investigating different parts of the Southern Weddell Sea.

1 Introduction

Coastal polynyas in the Antarctic are recurring areas of thin ice and open water, which are generally formed by divergent ice motion, e.g. by strong offshore winds or ocean currents. Polynyas are important hot spots for ice production, deep-water formation and gas ventilation of the ocean (e.g. Morales Maqueda et al., 2004).

TCD
9, 3959–3993, 2015

Due to the dependency of heat loss on the ice thickness (Maykut, 1978) and the nature of thermodynamic ice growth by release of latent heat at the ice/ocean interface, high rates of ice production occur predominately under thin-ice areas during austral winter (e.g. Tamura et al., 2011, 2007; Renfrew et al., 2002; Thorndike et al., 1975). The knowledge of ice production in polynyas is of large interest. Tamura et al. (2008) estimate that about 10 % of the Antarctic sea ice is produced within the major polynyas. However, direct measurements in the coastal polynyas are difficult and rare, which results in a lack of in-situ data.

In this study, the geographical focus lies on the Southern Antarctic Weddell Sea region between 69–78° S and 65–20° W (Fig. 1). With an average maximum winter extension of about 4.75×10^6 km^2, the Weddell Sea has the largest fraction of Antarctic sea-ice cover (Drucker et al., 2011).

The majority of recent studies dealing with polynya dynamics in this region make use of passive-microwave sensors. In comparison to thermal-infrared sensors, passive-microwave sensors retrieve data with no limitations due to day/night-time or clouds. Drucker et al. (2011) use SSM/I and AMSR-E data to derive ice-production rates and estimate ice export rates for the Weddell and Ross Seas in the years from 1992 to 2008. Kern (2009) derived pan-Antarctic coastal-polynya areas from SSM/I data for the same time period. Tamura et al. (2011) use SSM/I data to estimate surface heat and salt fluxes that are associated with sea-ice growth/melt in the Southern Ocean. Nihashi and Ohshima (2015) conducted a circumpolar mapping of polynya area and ice production based on passive-microwave as well as thermal-infrared remote sensing.

In this study, we present long-term results from coastal polynyas in the Southern Weddell Sea that were derived from Moderate-Resolution Imaging Spectroradiometer (MODIS) thermal-infrared imagery. Remote sensing of sea ice using thermal-infrared data yields the opportunity to monitor thin-ice thicknesses and distribution on a regular basis (Adams et al., 2013; Willmes et al., 2010; Yu and Rothrock, 1996). While the basic approach was used before in Arctic regions (e.g. Preußer et al., 2015; Adams et al., 2013; Willmes et al., 2011, 2010), we present now the first continuous and cloud-cover

TCD
9, 3959–3993, 2015

corrected time-series of polynya dynamics during the austral winter period (April to September) and for the complete coastal area in the Southern Weddell Sea for years from 2002 to 2014.

2 Data and methods

2.1 Input data

2.1.1 MODIS data (MOD/MYD29)

In this study we make use of the MODIS Sea Ice product (MOD/MYD29, Riggs et al., 2006; Hall et al., 2004), distributed by the US National Snow and Ice Data Centre (NSIDC). Our work is based on the ice-surface temperature data set (IST), which is one part of the sea-ice product. The provided data has a spatial resolution of 1 km × 1 km at nadir and each swath covers an area of 1354 km (across track) × 2030 km (along track) which equals approximately a time window of five minutes. The overall IST accuracy of the MOD/MYD29 sea-ice product under ideal (i.e. clear-sky) conditions is 1–3 K (Riggs et al., 2006; Hall et al., 2004). The MOD/MYD29 data product was already corrected for cloud cover using the MODIS cloud mask. We used this data for the austral winter period from 1 April to 30 September for the years from 2002 to 2014 that comprise a total of 141 056 MODIS swaths which cover the Southern Weddell Sea area.

2.1.2 ECMWF ERA-interim reanalysis

The set of input data is complemented by the European Centre of Medium Range Weather Forecast (ECMWF) ERA-Interim reanalysis data (Dee et al., 2011). The ERA-Interim data are distributed at a spatial resolution of 0.75° and were linearly interpolated to spatially and temporarily fit the MODIS data. For our analysis we used the 2 m air temperature, the 10 m wind-speed components, the mean sea-level pressure and the

TCD
9, 3959–3993, 2015

2 m dew-point temperature. These data sets supply all necessary input to calculate the energy balance for the thin-ice retrieval.

In addition to these meteorological variables, cloud-cover information was also taken from the ERA-Interim reanalysis data. In our case, we used the medium-level cloud-cover fraction data, which was found to show the in general best agreement with MODIS satellite data and the MODIS cloud mask during daytime (Liu and Key, 2014). This data set is used to complement the MODIS cloud mask during nighttime and was also spatially and temporarily interpolated to fit each MODIS swath.

2.2 Thin-ice retrieval

The derived thin-ice thickness (TIT) is calculated by using a simple surface-energy-balance and thermodynamic sea-ice model (Adams et al., 2013). This model utilizes the fact that the ice-surface temperature of thin ice decreases with increasing ice thickness (Drucker et al., 2003; Yu and Rothrock, 1996). Necessary assumptions comprise thin and snow-free sea ice, a linear temperature gradient throughout the ice and the temperature at the ice/ocean interface to be constant and at freezing point of sea water. In addition, all processing is carried out for nighttime only, to avoid dealing with short-wave radiation and snow/ice-albedo effects. The turbulent fluxes of sensible and latent heat as well as the long-wave radiation balance are calculated following Adams et al. (2013). For the flux calculation, the iterative stability-dependent bulk approach of Launiainen and Vihma (1990) is used. The long-wave radiation balance is calculated using an improved parametrization by Jin et al. (2006) for the downward long-wave radiation and the Stefan–Boltzman law for the upward long-wave radiation.

The exact procedure of the thin-ice thickness retrieval as well as all equations are thoroughly described in Adams et al. (2013). For ice-thickness classes between 0.0–0.2 m, Adams et al. (2013) state an average uncertainty of ±4.7 cm. Ice-thickness data above a 0.2 m threshold yield significantly higher uncertainties (Adams et al., 2013), which is why we limit our investigation accordingly.

TCD
9, 3959–3993, 2015

2.3 Data processing

2.3.1 Area of investigation and general procedure

For better comparison to other studies, the Southern Weddell Sea coastal area was divided into six sub regions (Fig. 1), namely from west to east: Antarctic Peninsula (AP), Ronne Ice Shelf (RO), the area around the grounded iceberg A23A (IB), Filchner Ice Shelf (FI), Coats Land (CL) and the Brunt Ice Shelf (BR).

All MODIS swaths were processed in several steps as visualized in Fig. 2. First, all MODIS swaths along with the ERA-Interim data sets were projected onto a common grid using a nearest-neighbor approach. No interpolation was applied. Subsequently, TIT is calculated pixel-wise and daily median-TIT composites are calculated. These composites comprise TIT and IST data alongside the daily energy-balance components of each thin-ice pixel. In the next step, cloud-covered data was identified and corrected as will be described in the following subsections.

2.3.2 Identification of low quality data

We use ERA-Interim medium-level cloud-cover information to reduce the influence of cloud-affected pixels in the aggregation process of the daily TIT composites. We apply a simple cloud-cover threshold (75 %) to identify cloud covered regions from ERA-Interim data and thereby provide an additional indicator to the MODIS cloud mask for an identification of potentially cloud-affected pixels. This data is also aggregated into daily composites and separated into four different cloud-cover dependent classes (Fig. 2). Pixels that are considered as clear-sky by means of the MODIS cloud mask as well as the ERA-Interim cloud-cover information for all available daily swaths, are assigned to the confident clear-sky class (ccs). In contrast, pixels that feature cloud cover in both data sets for all available swaths are assigned to the definite cloud-cover class (dcc). All pixels that show a mix of cloud-covered and clear-sky conditions are assigned to the mixed-covered pixel class (mcp) with a clear-sky index based upon the

TCD
9, 3959–3993, 2015

ratio of the number of clear-sky input swaths to the total number of input swaths. Pixels that are not covered by any swath during one day are assigned to the uncovered pixel class (ucp).

In order to reduce the inherent misclassification problems of the MODIS cloud mask with clouds taken for either thin or thick ice, we introduced an additional procedure that assigns a persistence index (PIX, Fig. 2). Hereby, we make use of the temporal and spatial persistence of the temperature signal in polynyas in contrast to mobile cloud patterns. The persistence index is the ratio of the number of swaths per pixel that contain thin ice (TIT$\leq$ 0.2 m) to the total number of clear-sky acquisitions covering that pixel.

2.3.3 Correction scheme for cloud-covered data

Employing the above mentioned two procedures, we are able to identify low-quality data. These are then accounted for by a two-step procedure: first, we apply the spatial feature reconstruction (SFR) approach introduced in Paul et al. (2015). The remaining coverage gaps that could not be corrected for by this approach, e.g. due to temporal gaps longer than three consecutive days, we use the proportional extrapolation (PE) scheme as used and described by Preußer et al. (2015). This way, we achieve full cloud-cover correction by minimizing the drawbacks of solely using proportional extrapolation. In the rare case, that no coverage above 50 % can be achieved with the SFR approach, the day will be interpolated between neighboring days with sufficient (i.e. above 50 %) coverage.

In the SFR approach, the information of the surrounding six days (three before and three after the initial day of interest, respectively) is weighted directly proportional with their temporal proximity to the initial daily median composite, which yields a probability of thin-ice occurrence. A detailed description and analysis of the SFR approach and its setup is given in Paul et al. (2015). The PE approach assigns thin ice to cloud-covered areas in the same proportion as it is detected in the cloud-free area. For example, if

TCD
9, 3959–3993, 2015

a region is 80 % cloud free and 50 % of this area features a thin-ice signal, then 50 % of the cloud-covered region is considered as thin ice.

We complemented the resulting binary information from the SFR approach (i.e. thin-ice or no thin ice) with a pixel-wise median ice-thickness and ice-surface temperature value of the surrounding days (TIT_{add}/IST_{add}, Fig. 2).

2.3.4 Derived output polynya parameters

We derive daily polynya area (POLA) as well as the accumulated winter-time ice-production (IP) from heat loss (e.g. Tamura et al., 2011; Willmes et al., 2011) for each POLA pixel.

$$\frac{\partial h}{\partial t} = \frac{Q_\mathrm{i}}{\rho_\mathrm{i}\, L_\mathrm{f}} \tag{1}$$

Assuming that the complete heat loss through the ice (Q_i, Eq. 1) contributes to new ice formation ($\frac{\partial h}{\partial t}$), the volume ice production rate $\frac{\partial V}{\partial t}$ can be calculated by multiplying $\frac{\partial h}{\partial t}$ with the spatial extent of each POLA pixel. In Eq. (1), we assume a sea-ice density (ρ_i) of 910 kg m^{-3} and the latent heat of fusion (L_f) for sea ice to be 3.44×10^5 J kg^{-1}.

Furthermore, thin-ice thickness distributions as well as frequency distributions of thin-ice occurrence were calculated. The results will then be put in context with other recent remote sensing and model studies.

3 Results and discussion

3.1 Cloud-cover corrections

The MODIS coverage without cloud-cover correction is roughly between 40 and 100 % due to the high amount of daily swaths that at least partially cover a large region like the Southern Weddell Sea. The use of the spatial feature reconstruction approach (SFR,

TCD
9, 3959–3993, 2015

Paul et al., 2015) can mitigate the effect of cloud cover to a great extent yet not completely. At the same time, this is done with high confidence that no thin ice is randomly added in areas where a polynya is unlikely to appear, which can potentially happen when solely using proportional extrapolation (PE, Preußer et al., 2015). However, to achieve full coverage the additional use of PE is necessary.

An average of 78 % in all MODIS composites per day over all six sub regions is classified as cloud free. After the application of the SFR approach, we achieve an average coverage of 97 % per day, where the remaining 3 % get corrected for by PE.

When comparing our two-step cloud-cover correction procedure to the sole use of proportional extrapolation (Table 1), we find that the latter one yields generally higher correction estimates for the three smaller regions (IB, FI and CL) as well as for the Antarctic Peninsula region. However, this observation is reversed for the highly active regions in front of the Ronne Ice Shelf (RO) and the Brunt Ice Shelf (BR). Here, the sole use of PE results in lower estimates. Especially in spatially large regions with low polynya activity like the Antarctic Peninsula (PA, Fig. 4) sole use of PE reveals its disadvantage by more than doubling the uncorrected value (RAW, Table 1).

We mentioned before that whenever no coverage above 50 % can be achieved, the POLA information of that day will be interpolated between days with sufficient (i.e. above 50 %) coverage. Under the same premise, the PE approach is used for comparison to the two-step procedure (SFR + PE, Table 1). However, when solely applying the PE approach, interpolation is necessary on average on 34 occasions per year and region due to present cloud coverage in the MODIS composites. With the use of the SFR approach, interpolation is on average only necessary on two days per year and region. The use of SFR potentially leads a decrease uncertainties, especially when investigating single days.

3.2 Thin-ice thickness and frequency distribution

The overall distribution of thin-ice thicknesses for the Southern Weddell Sea (Fig. 3) does not show strong regional nor seasonal differences as can be seen from the low

TCD
9, 3959–3993, 2015

standard deviations. However, the standard deviations are larger for the smallest and largest thickness classes. In general, the thin-ice thickness distribution features a steep increase of occurrences from smaller to larger thickness classes.

Almost the complete coastal area in the South and East of the investigated Southern Weddell Sea features a recurrent thin-ice signal for the years from 2002 to 2014 (around 30 % and above, Fig. 4). The overall high recurrence of thin ice is a very important note when considering that the primary focus of many studies lies solely on the Ronne Ice Shelf (RO) region when investigating the Weddell Sea (e.g. Nihashi and Ohshima, 2015). This neglects the importance of e.g. the Brunt Ice Shelf (BR) region to the overall ice production and ocean-atmosphere exchange. It also underestimates the contribution of the area around the grounded iceberg A23A (IB), Filchner Ice Shelf (FI) and Coats Land (CL) to the bottom-water formation due to salt release during ice formation.

The relative frequency of thin-ice occurrences in the Antarctic Peninsula (AP) region is spatially focused around smaller grounded icebergs and rather low compared to the other sub regions. The very light blue areas in the northeast of the investigation area correspond to a low sea-ice concentration area due to the far south lying marginal ice zone (MIZ) in April in the years 2005 and 2006 near the Brunt Ice Shelf region (at around 75° S, taken from AMSR-E observations, not shown). However, those two years can most likely not solely explain the increased frequency of thin-ice occurrences in the central Southern Weddell Sea. There is a sharp separation from this zone with present activity in the North and North-East to a zone with almost no activity in the South and South-West closer to the Ronne and Filchner Ice Shelves. This line of separation (Fig. 4, A) coincides very well with the course of the continental slope (Fig. 1, Arndt, 2013), but no conclusive explanation can be given.

Markus (1996) studied the effect of the grounded ice berg A23A on the ice production in front of the Filchner Ice Shelf and found a drastic average increase in sea-ice concentration (i.e. a decrease in the amount of thin-ice area and hence ice production) during the freezing period. While the recurring formation of a fast-ice bridge is also visible in

TCD
9, 3959–3993, 2015

our results (a low frequency area between the coast and the grounded iceberg A23A, Fig. 4, B), we still find high polynya activity in front of Coats Land (CL) and the Filchner Ice Shelf (FI). Also the area around the grounded iceberg A23A (IB) and the westward side of the ice bridge show high thin-ice occurrences. Our frequency estimates for the Ronne Ice Shelf (RO) region between 30 and 40 % are in good agreement with the results found in Nihashi and Ohshima (2015).

3.3 Polynya area and ice production

Results for polynya area (POLA) and ice production (IP) for the years from 2002 to 2014 between 1 April and 30 September are presented in Figs. 5 and 6, respectively. The investigated six sub regions can be divided into two classes: the highly active Ronne Ice Shelf (RO, Fig. 5b) and Brunt Ice Shelf (BR, Fig. 5f) regions with also a large contribution in ice production (Fig. 6b and f) and the smaller contributors of Antarctic Peninsula (AP, Figs. 5 and 6a), iceberg A23A (IB, Figs. 5 and 6c), Filchner Ice Shelf (FI, Figs. 5 and 6d) and Coats Land (CL, Figs. 5 and 6e). All regions show a high inter-annual variability.

We find a decrease in average seasonal POLA and hence also in accumulated ice production in the most recent years for the Ronne Ice Shelf region (RO, Figs. 5 and 6b). While the 13 year trend is not significant, the 10 year POLA trend (2005–2014) is significant given a level of significance of $\alpha = 5\,\%$ with a decrease of $347.60\,\mathrm{km^2 a^{-1}}$. Generally, by means of multi-year trends over the course of 13 years in POLA and IP (Figs. 5 and 6), all regions except Coats Land (CL) exhibit a negative trend for both POLA and IP.However, not all of those trends are statistically significant. AP shows a significant trend ($\alpha = 5\,\%$) with approx. $-741\,\mathrm{km^2}$ and $-7\,\mathrm{km^3}$ respectively. The region around the grounded iceberg A23A (IB) also features a multi-year negative significant trend in POLA with approx. $-858\,\mathrm{km^2}$.

Another important fact that is shown by our data set is the importance of the Filchner Ice Shelf (FI) and Coats Land (CL) region. Together with the area around the grounded iceberg A23A (IB), each shows a higher average POLA and IP than the Antarctic Penin-

TCD
9, 3959–3993, 2015

sula (AP) region. However, the inter-annual variability is very high, especially in the IB and FI region. The combined average POLA of IB, FI and CL is in the same order of magnitude as the larger contributors of Ronne and Brunt Ice Shelf (RO and BR, Figs. 5 and 6). This also holds for the ice production. Without the IB region, FI and CI show an average polynya area of 1400 km^2 and accumulated seasonal ice production of 15 km^3.

The frequency of days passing a certain polynya area threshold is shown in Fig. 7. This underlines again the high activity in the Ronne (Fig. 7b) and Brunt Ice Shelf (Fig. 7f) regions compared to the four less active regions. In more than 50 % of the investigated 2379 days, a polynya area larger than 1000 km^2 is present in front of the Brunt Ice Shelf. The same is true for 50 % of the investigated days in the Ronne Ice Shelf region and more than 25 % of the investigated days for the area around iceberg A23A.

A threshold of 8000 and 9000 km^2 is passed in 10 % of all observed days from 2002 to 2014 (April to September) in the Ronne Brunt Ice Shelf (RO) and Brunt Ice Shelf (BR) region, respectively.

Annual average polynya days (Fig. 8) reveal additional information on the temporal distribution of polynya dynamics (Fig. 7). For example, appearances of POLA values above 10 000 km^2 for the Filchner Ice Shelf (FI, Fig. 8d) region are mainly focused on the year 2003. Here, about one third of found polynyas feature a polynya area above 10 000 km^2. The inter-annual variability in polynya-size distribution per day is also quite high in other regions, especially in the Ronne Ice Shelf (RO) and Brunt Ice Shelf (BR) regions as well as in the area surrounding the grounded iceberg A23A (IB). Years with much higher than average annual POLA values (Fig. 5) also show a high amount of days with polynya days in the > 10 000 km^2 class.

The seasonal average polynya area (POLA) and the seasonal accumulated ice production (IP) are compared to the results from Haid and Timmermann (2013) in Figs. 9 and 10. Haid and Timmermann (2013) use the Finite-Element Sea-ice Ocean Model (FESOM) coupled with a dynamic-thermodynamic sea-ice model to derive polynya area and ice-production rates. Their data set covers the austral winter period from May

TCD
9, 3959–3993, 2015

to September for the years from 1990 to 2009. Due different investigation intervals and sub regions, we excluded the April data and focused on the Antarctic Peninsula (AP), Ronne Ice Shelf (RO) and the Brunt Ice Shelf (BR) for the period from May to September in compliance with the model estimates from Haid and Timmermann (2013).

For the Antarctic Peninsula region (AP), the model estimates are consistently higher than our results (Figs. 9 and 10). A general reason for this is the use of the NCEP reanalysis data (Kalnay et al., 1996). Especially the narrow mountain range of the Antarctic Peninsula is not sufficiently represented in the atmospheric reanalysis data. Compared to high-resolution simulations, NCEP data show much higher wind speeds at the Antarctic Peninsula (Haid et al., 2015). Topographic effects on the wind such as katabatic winds and barrier winds influence a broader region due to the smoothed topography in NCEP. Hence, wind induced coastal polynya formation cannot be reproduced, particularly in the Antarctic Peninsula region. This presumably leads to overall unrealistically high POLA estimates and hence ice-production rates in the study from Haid and Timmermann (2013) for the AP region.

Focusing on polynya-area comparison for the two sub regions RO and BR (Fig. 9b and c), the presented comparison shows that the MODIS estimates exceed the model estimates every year with the exception of 2002/2003 for the Ronne Ice Shelf region (Fig. 9b). However, the extent of that difference can change a lot between each year and sub region. For the years from 2004 to 2009 in the Brunt Ice Shelf region, while our results again exceed the model estimates, the pattern of years with relative high/low POLA is equal between our results and the model estimates from Haid and Timmermann (2013). For the remaining years, no apparent similarities are present.

By means of ice production, estimates for the Ronne Ice Shelf (RO) as well as the Brunt Ice Shelf (BR) region are in the same order of magnitude and oftentimes very similar (with the exception of the years 2002 and 2003 for RO, Fig. 10). Generally, the model estimates are expected to be smaller than comparable satellite-derived results due to the negligence of the oceanic heat flux in our method. However, the opposite can be seen for the Southern Weddell Sea and especially for the Brunt Ice Shelf region.

TCD
9, 3959–3993, 2015

Assuming that the satellite-based estimates represent the upper limit for ice production, the model estimates (Haid and Timmermann, 2013) result from a higher ice production per polynya area compared to our results, which likely depends on the computation of the atmospheric heat fluxes.

The comparison of different studies is difficult due to differing investigation periods, diversity in spatial extent of used POLA masks as well as varying methods and changes in atmospheric forcing. For the following comparison of our results with several recent studies and investigations of the Southern Weddell Sea (Tables 2 and 3), we tried to match the used investigation period and regional extent in the best possible way.

Based on average seasonal polynya area (Table 2), we find the best agreement with POLA estimates of Nihashi and Ohshima (2015). The estimates are based on the period from May to August for the years 2003 to 2011 and are acquired from AMSR-E data. A general problem with passive-microwave data is that it can be problematic to distinguish between the signals from adjacent icebergs, fast ice or ice shelves and the thin-ice signal of coastal polynyas (Tamura et al., 2008). Hence, algorithms based on passive-microwave sensor data can only resolve relatively large polynyas while fairly narrow coastal polynyas, like those in the Weddell Sea, may remain undetected (Tamura et al., 2007).

Our multi-year averages exceed the results from Haid and Timmermann (2013) in the Ronne Ice Shelf region and especially in the Brunt Ice Shelf region. For the Antarctic Peninsula region our results are much lower than the model estimates. The good agreement in results between our study and Nihashi and Ohshima (2015) and the differences to Haid and Timmermann (2013) are also potentially related to different atmospheric forcing (Haid et al., 2015).

Kern (2009) did not separate the Weddell Sea into different sub regions, but just gave a POLA estimate for the complete region and for a longer investigation period from 1992–2008. In this study also some areas in the Northern Antarctic Peninsula were included that were not covered in our study. The larger spatial extent together with the longer investigation period, which is supposedly coined by a negative long-term trend

TCD
9, 3959–3993, 2015

(e.g. Drucker et al., 2011; Tamura et al., 2008), prohibits a serious comparison and might also explain the big difference in average POLA.

The comparison of ice production between ours and other recent studies in the Southern Weddell Sea (Table 3) reveals that the model results (Haid and Timmermann, 2013) for the Antarctic Peninsula are again much higher than our estimates. In the remaining two regions, the MODIS results exceed the model estimates in the BR region, but are lower in the RO region, which results from the differences in IP for the years 2002 and 2003.

Drucker et al. (2011) found in their study based on AMSR-E 12.5 km × 12.5 km 36 GHz data for the years 2003 to 2008 and for a slightly longer investigation period from April to October an average of 99 km^3 for the Ronne Ice Shelf, 112 km^3 for the Brunt Ice Shelf and 30 km^3 for the region around the grounded iceberg A23A. These estimates are much higher than our results by almost triple the ice production in each of the three investigated regions (Table 3). This effect is very unlikely to be solely based on the additional month used in the investigation period. However, in the study by Nihashi and Ohshima (2015) a comparison between ice production from AMSR-E and SSM/I with regard to the spatial resolution of the sensors showed that lower spatial resolution oftentimes goes along with higher estimates of ice production. Estimates from SSM/I are likely to exceed the results based on AMSR-E data with a much higher resolution (12.5 vs. 6.25 km^2, respectively). In the Ronne Ice Shelf region, the difference between SSM/I and AMSR-E is especially large (42 km^3 for AMSR-E compared to 71 km^3 for SSM/I, Nihashi and Ohshima, 2015 based upon Tamura et al., 2011). Given an increase in resolution due to the here used MODIS data compared to the low resolution of the AMSR-E 36 GHz channel used by Drucker et al. (2011), this might explain our overall lower results to some extent. Additionally, Drucker et al. (2011) stated an error margin of their results of ±30 %.

Similar to the POLA results, the most recent study by Nihashi and Ohshima (2015) for the years 2003 to 2010 again shows the best agreement with our results (Table 3). While their study is also based on a slightly longer wintertime investigation period from

TCD
9, 3959–3993, 2015

April to October, the increase in ice production for October is more in line with expectations compared to Drucker et al. (2011).

3.4 Energy-balance components

The mean seasonal area-weighted atmospheric fluxes are shown in Fig. 11 based upon the here-used three components of turbulent fluxes of sensible (H) and latent heat (E) as well as the long-wave radiation balance (L^*). Short-wave radiation was omitted due to the stated limitation to only use nighttime MODIS swaths for the thin-ice retrieval. The estimates from Haid and Timmermann (2013) were adjusted accordingly and also only show these three components.

As expected, we find the sensible heat flux to be the largest contributor to the total atmospheric flux (e.g. Maykut, 1978). The inter-annual variability is rather low for the Brunt Ice Shelf (BR) and the Ronne Ice Shelf (RO) region, while it is comparatively pronounced for the Antarctic Peninsula (AP). Regional differences are present, but they are rather low in comparison to the model estimates from Haid and Timmermann (2013). Overall, the results of Haid and Timmermann (2013) exceed ours, especially in the Ronne Ice Shelf (RO) region. The discrepancy in the Antarctic Peninsula region is most likely again related to the use of NCEP atmospheric reanalysis data (Kalnay et al., 1996).

We stated earlier that the model estimates seem to achieve a higher ice production per polynya area compared to the MODIS-derived results. An explanation can be found in the work of Lindsay et al. (2014). In their study, Lindsay et al. (2014) compared seven different atmospheric reanalysis products against each other and with observational data in the Arctic. The results indicate a large negative bias in 2 m air temperature (more than 2 K) in the NCEP reanalysis data (Kalnay et al., 1996) compared to observational data as well as the ERA-Interim reanalysis data (Dee et al., 2011) used in our study. The on average much colder air temperatures in the NCEP data drastically increase the sensible heat flux to the atmosphere.

TCD
9, 3959–3993, 2015

Renfrew et al. (2002) found in their study for the years 1992–1998 and using an adaptive, in general much longer freezing period (roughly from February to November) a contribution of 63, 22, and 15 % for the sensible, latent and radiative components of the atmospheric heat flux, respectively. The average contribution to the total atmospheric flux amounts to 56, 7 and 37 % for the sensible, latent and long-wave radiative components in our results. In our data as well as in the results from Haid and Timmermann (2013), the long-wave radiation shows an on average higher contribution to the total atmospheric flux than in the study of Renfrew et al. (2002). Our average freezing season area-integrated energy exchange with the atmosphere amounts to 7.04×10^{18} J compared to 3.48×10^{19} J in Renfrew et al. (2002). However, Renfrew et al. (2002) used a much longer freezing period. Additionally, there is no temporal overlap between our study and the work of Renfrew et al. (2002), which makes an inter-comparison very difficult.

4 Summary and conclusion

In this study, we present a data set of MODIS-derived polynya-area estimates and ice-production rates as well as thin-ice frequency distribution, thin-ice thickness distribution and energy-balance components for the Southern Weddell Sea, Antarctica. This was done for a 13 year time interval (2002 to 2014) during the austral winter period from April to September for the complete coastal area separated into six sub regions. For that, we utilized the higher spatial resolution of MODIS compared to passive microwave sensors such as SSM/I and AMSR-E/AMSR2. The addition of a more strict exclusion of cloud-covered data using ERA-Interim data to the established thin-ice retrieval as well as the adaptation of a new approach to compensate for cloud-covered areas in daily MODIS composites is presented and discussed.

The data set is unique in a way that it is the first long-term investigation of polynya dynamics based on cloud-cover corrected thermal-infrared data that covers the complete Southern Weddell Sea coastal area. The results were discussed in comparison to re-

TCD
9, 3959–3993, 2015

cently published studies using a variety of different methods and approaches (satellite sensors and models). On average over 13 years, we find the sea-ice areas in front of Ronne and Brunt Ice Shelf to be the most active with an annual average polynya area of 3018 ± 1298 and $3516 \pm 1420\,km^2$ as well as an accumulated volume ice production of 31 ± 13 and $31 \pm 12\,km^3$, respectively. Especially the Ronne Ice Shelf polynya is very important for the bottom-water formation. For the remaining four regions, our estimates amount to $421 \pm 294\,km^2$ and $4 \pm 3\,km^3$ (Antarctic Peninsula), $1148 \pm 432\,km^2$ and $12 \pm 5\,km^3$ (Iceberg A23A), $901 \pm 703\,km^2$ and $10 \pm 8\,km^3$ (Filchner Ice Shelf) as well as $499 \pm 277\,km^2$ and $5 \pm 2\,km^3$ (Coats Land).

Given these results and also the presented thin-ice frequency distribution, the neglect of certain regions in other studies, namely the area around the grounded iceberg A23A as well as the area off the coast of the Filchner Ice Shelf and Coats Land, showed up to drastically underestimate the total average polynya area and ice production in the Southern Weddell Sea. Together, all three regions contribute comparably to the most active regions in front of Ronne and Brunt Ice Shelf. These regions should be further investigated by upcoming studies as they also contribute to the bottom-water formation. The data set of this study will be made available on PANGAEA shortly after publication.

Acknowledgements. The study was funded by the Deutsche Forschungs Gemeinschaft in the framework of the priority program SPP1158 “Antarctic Research with comparative investigations in Arctic ice areas” by grant HE2740/12. The authors want to thank the National Snow and Ice Data Center and the European Centre for Medium-Range Weather Forecasts for the provision of the here-used data. The authors appreciate the help of Verena Haid and Ralph Timmermann by providing FESOM model results.

TCD
9, 3959–3993, 2015

References

Adams, S., Willmes, S., Schröder, D., Heinemann, G., Bauer, M., and Krumpen, T.: Improvement and sensitivity analysis of thermal thin-ice thickness retrievals, IEEE T. Geosci. Remote, 51, 3306–3318, 2013. 3961, 3963

Arndt, J. E.: The International Bathymetric Chart of the Southern Ocean (IBCSO) – Digital Bathymetric Model, Alfred Wegener Institute, Helmholtz Center for Polar and Marine Research, Bremerhaven, doi:10.1594/PANGAEA.805734, 2013. 3968, 3983

Dee, D. P., Uppala, S. M., Simmons, A. J., Berrisford, P., Poli, P., Kobayashi, S., Andrae, U., Balmaseda, M. A., Balsamo, G., Bauer, P., Bechtold, P., Beljaars, A. C. M., van de Berg, L., Bidlot, J., Bormann, N., Delsol, C., Dragani, R., Fuentes, M., Geer, A. J., Haimberger, L., Healy, S. B., Hersbach, H., Hólm, E. V., Isaksen, L., Kållberg, P., Köhler, M., Matricardi, M., McNally, A. P., Monge-Sanz, B. M., Morcrette, J.-J., Park, B.-K., Peubey, C., de Rosnay, P., Tavolato, C., Thépaut, J.-N., and Vitart, F.: The ERA-Interim reanalysis: configuration and performance of the data assimilation system, Q. J. Roy. Meteorol. Soc., 137, 553–597, doi:10.1002/qj.828, 2011. 3962, 3974

Drucker, R., Martin, S., and Moritz, R.: Observations of ice thickness and frazil ice in the St. Lawrence Island polynya from satellite imagery, upward looking sonar, and salinity/temperature moorings, J. Geophys. Res., 108, 3149, doi:10.1029/2001JC001213, 2003. 3963

Drucker, R., Martin, S., and Kwok, R.: Sea ice production and export from coastal polynyas in the Weddell and Ross Seas, Geophys. Res. Lett., 38, L17502, doi:10.1029/2011GL048668, 2011. 3961, 3973, 3974, 3982

Haid, V. and Timmermann, R.: Simulated heat flux and sea ice production at coastal polynyas in the southwestern Weddell Sea, J. Geophys. Res.-Oceans, 118, 2640–2652, doi:10.1002/jgrc.20133, 2013. 3970, 3971, 3972, 3973, 3974, 3975, 3981, 3982, 3991, 3993

Haid, V., Timmermann, R., Ebner, L., and Heinemann, G.: Atmospheric forcing of coastal polynyas in the south-western Weddell Sea, Antarct. Sci., 27, 388–402, doi:10.1017/S0954102014000893, 2015. 3971, 3972

Hall, D., Key, J., Casey, K., Riggs, G., and Cavalieri, D.: Sea ice surface temperature product from MODIS, IEEE T. Geosci. Remote, 42, 1076–1087, doi:10.1109/TGRS.2004.825587, 2004. 3962

TCD
9, 3959–3993, 2015

Jin, X., Barber, D., and Papakyriakou, T.: A new clear-sky downward longwave radiative flux parameterization for Arctic areas based on rawinsonde data, J. Geophys. Res., 111, D24104, doi:10.1029/2005JD007039, 2006. 3963

Kalnay, E., Kanamitsu, M., Kistler, R., Collins, W., Deaven, D., Gandin, L., Iredell, M., Saha, S., White, G., Woollen, J., Zhu, Y., Leetmaa, A., Reynolds, R., Chelliah, M., Ebisuzaki, W., Higgins, W., Janowiak, J., Mo, K. C., Ropelewski, C., Wang, J., Jenne, R., and Joseph, D.: The NCEP/NCAR 40-year reanalysis project, B. Am. Meteorol. Soc., 77, 437–471, doi:10.1175/1520-0477(1996)077<0437:TNYRP>2.0.CO;2, 1996. 3971, 3974

Kern, S.: Wintertime Antarctic coastal polynya area: 1992–2008, Geophys. Res. Lett., 36, L14501, doi:10.1029/2009GL038062, 2009. 3961, 3972, 3981

Launiainen, J. and Vihma, T.: Derivation of turbulent surface fluxes an iterative flux-profile method allowing arbitrary observing heights, Environ. Softw., 5, 113–124, doi:10.1016/0266-9838(90)90021-W, 1990. 3963

Lindsay, R., Wensnahan, M., Schweiger, A., and Zhang, J.: Evaluation of seven different atmospheric reanalysis products in the Arctic, J. Climate, 27, 2588–2606, doi:10.1175/JCLI-D-13-00014.1, 2014. 3974

Liu, Y. and Key, J. R.: Less winter cloud aids summer 2013 Arctic sea ice return from 2012 minimum, Environ. Res. Lett., 9, 044002, doi:10.1088/1748-9326/9/4/044002, 2014. 3963

Markus, T.: The effect of the grounded tabular icebergs in front of Berkner Island on the Weddell Sea ice drift as seen from satellite passive microwave sensors, in: International Geoscience and Remote Sensing Symposium, 1996, IGARSS '96, "Remote Sensing for a Sustainable Future", vol. 3, Lincoln, NE, 1791–1793, 1996. 3968

Maykut, G. A.: Energy exchange over young sea ice in the central Arctic, J. Geophys. Res., 83, 3646–3658, doi:10.1029/JC083iC07p03646, 1978. 3961, 3974

Morales Maqueda, M. A., Willmott, A. J., and Biggs, N. R. T.: Polynya dynamics: a review of observations and modeling, Rev. Geophys., 42, RG1004, doi:10.1029/2002RG000116, 2004. 3960

Nihashi, S. and Ohshima, K. I.: Circumpolar mapping of Antarctic coastal polynyas and landfast sea ice: relationship and variability, J. Climate, 28, 3650–3670, doi:10.1175/JCLI-D-14-00369.1, 2015. 3961, 3968, 3969, 3972, 3973, 3981, 3982

Paul, S., Willmes, S., Gutjahr, O., Preußer, A., and Heinemann, G.: Spatial feature reconstruction of cloud-covered areas in daily MODIS composites, Remote Sensing, 7, 5042–5056, 2015. 3965, 3967, 3980, 3984

TCD
9, 3959–3993, 2015

Preußer, A., Willmes, S., Heinemann, G., and Paul, S.: Thin-ice dynamics and ice production in the Storfjorden polynya for winter seasons 2002/2003–2013/2014 using MODIS thermal infrared imagery, The Cryosphere, 9, 1063–1073, doi:10.5194/tc-9-1063-2015, 2015. 3961, 3965, 3967, 3980, 3984

Renfrew, I. A., King, J. C., and Markus, T.: Coastal polynyas in the southern Weddell Sea: variability of the surface energy budget, J. Geophys. Res., 107, 3063, doi:10.1029/2000JC000720, 2002. 3961, 3975

Riggs, G., Hall, D., and Salomonson, V.: MODIS Sea Ice Products User Guide to Collection 5, National Snow and Ice Data Center, University of Colorado, Boulder, CO, USA, 2006. 3962

Tamura, T., Ohshima, K. I., Markus, T., Cavalieri, D. J., Nihashi, S., and Hirasawa, N.: Estimation of thin ice thickness and detection of fast ice from SSM/I data in the Antarctic ocean, J. Atmos. Ocean. Tech., 24, 1757–1772, doi:10.1175/JTECH2113.1, 2007. 3961, 3972

Tamura, T., Ohshima, K. I., and Nihashi, S.: Mapping of sea ice production for Antarctic coastal polynyas, Geophys. Res. Lett., 35, L07606, doi:10.1029/2007GL032903, 2008. 3961, 3972, 3973

Tamura, T., Ohshima, K. I., Nihashi, S., and Hasumi, H.: Estimation of surface heat/salt fluxes associated with sea ice growth/melt in the Southern ocean, Scient. Online Lett. Atmos., 7, 17–20, 2011. 3961, 3966, 3973

Thorndike, A. S., Rothrock, D. A., Maykut, G. A., and Colony, R.: The thickness distribution of sea ice, J. Geophys. Res., 80, 4501–4513, doi:10.1029/JC080i033p04501, 1975. 3961

Willmes, S., Krumpen, T., Adams, S., Rabenstein, L., Haas, C., Hoelemann, J., Hendricks, S., and Heinemann, G.: Cross-validation of polynya monitoring methods from multisensor satellite and airborne data: a case study for the Laptev Sea, Can. J. Remote Sens., 36, S196–S210, doi:10.5589/m10-012, 2010. 3961

Willmes, S., Adams, S., Schröder, D., and Heinemann, G.: Spatio-temporal variability of polynya dynamics and ice production in the Laptev Sea between the winters of 1979/80 and 2007/08, Polar Res., 30, 5971, doi:10.3402/polar.v30i0.5971, 2011. 3961, 3966

Yu, Y. and Rothrock, D. A.: Thin ice thickness from satellite thermal imagery, J. Geophys. Res., 101, 25753–25766, doi:10.1029/96JC02242, 1996. 3961, 3963

TCD
9, 3959–3993, 2015

Table 1. Comparison between uncorrected MODIS data (RAW), sole use of proportional extrapolation (PE, Preußer et al., 2015) and a combined step-wise approach using both, spatial feature reconstruction (SFR, Paul et al., 2015) and proportional extrapolation. Values are presented for each of the six sub regions (Fig. 1) and based on their multi-year average polynya area [km^2].

	AP	RO	IB	FI	CL	BR
RAW	351	2567	1030	815	451	2956
SFR + PE	421	3018	1148	901	499	3516
PE	758	2835	1259	1013	659	3250

TCD
9, 3959–3993, 2015

Table 2. Summary of average polynya-area estimates [km^2] from various studies (Haid and Timmermann (2013) (HT13); Kern (2009) (K09); as well as Nihashi and Ohshima (2015) (NO15)). Corresponding results of this study are given in parenthesis. MODIS estimates vary between studies due to different sample intervals of each comparison study we tried to match in the best possible way. Kern (2009) did only give an estimate for the complete Southern and Western Weddell Sea.

Study	AP	RO	BR
HT13	1706 (488)	1961 (3482)	924 (2772)
K09		21 200 (11 158)	
NO15	–	2300 (3520)	–

TCD
9, 3959–3993, 2015

Table 3. Summary of accumulated volume ice-production estimates [km^3] from various studies (Haid and Timmermann (2013) (HT13); Drucker et al. (2011) (D11); as well as Nihashi and Ohshima (2015) (NO15)). Corresponding results of this study are given in parenthesis. MODIS estimates vary between studies due to different sample intervals of each comparison study we tried to match in the best possible way.

Study	AP	RO	IB	BR
HT13	19 (4)	42 (30)	–	11 (20)
D11	–	99 (38)	30 (13)	112 (36)
NO15	–	38 (35)	–	–

TCD
9, 3959–3993, 2015

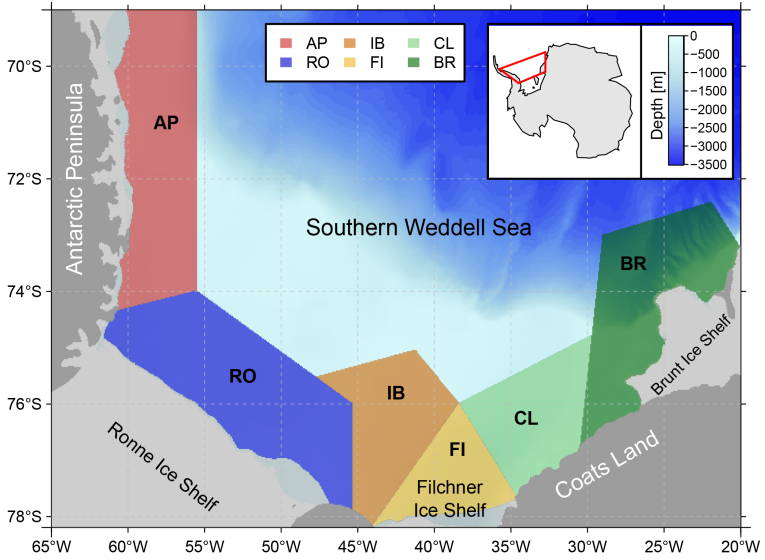

Figure 1. Sketch of the study area in the Southern Weddell Sea with all six investigated sub regions along the coast: Antarctic Peninsula (AP), Ronne Ice Shelf (RO), the area around the grounded iceberg A23A (IB), Filchner Ice Shelf (FI), Coats Land (CL) and the Brunt Ice Shelf (BR). Color shadings show the bathymetry based on Arndt (2013).

TCD
9, 3959–3993, 2015

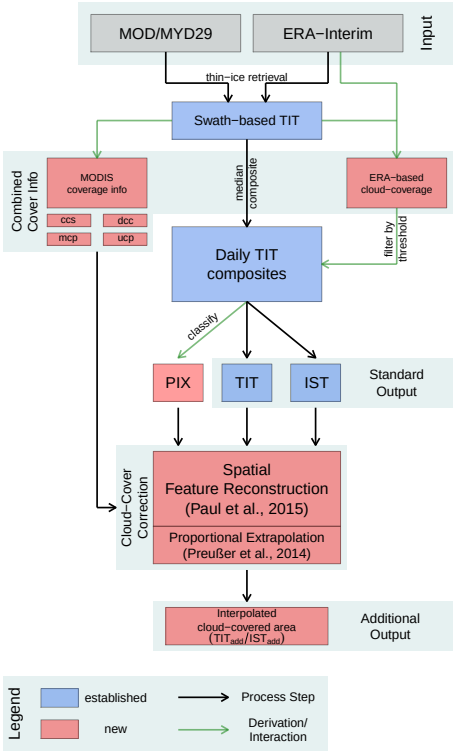

Figure 2. Work flow based on the described input data and thin-ice retrieval. Established processing steps, that were already used in other studies are marked in blue, while new additions are marked in red. These additions comprise a persistence index (PIX), the newly defined combined cloud-cover information of MODIS cloud mask and ERA-Interim medium-level cloud cover. Missing data due to cloud cover is accounted for by a two-step procedure that comprises spatial feature reconstruction (Paul et al., 2015) and proportional extrapolation (Preußer et al., 2015). The combined cloud-cover information separates between confident clear-sky (ccs), definite cloud-cover (dcc), mixed-covered pixels (mcp) and uncovered pixels (ucp).

TCD
9, 3959–3993, 2015

Long-term polynya dynamics from MODIS thermal-infrared imagery

S. Paul et al.

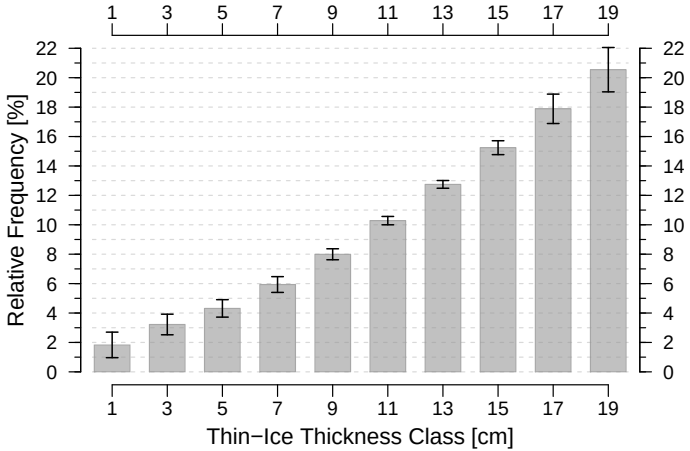

Figure 3. Averaged distribution of thin-ice thicknesses in the Southern Weddell Sea over the whole 13 year time interval between April and September. The class width is 2 cm, i.e. the 1 cm class includes thicknesses beween 0 and 2 cm. Error bars represent ± one standard deviation.

TCD
9, 3959–3993, 2015

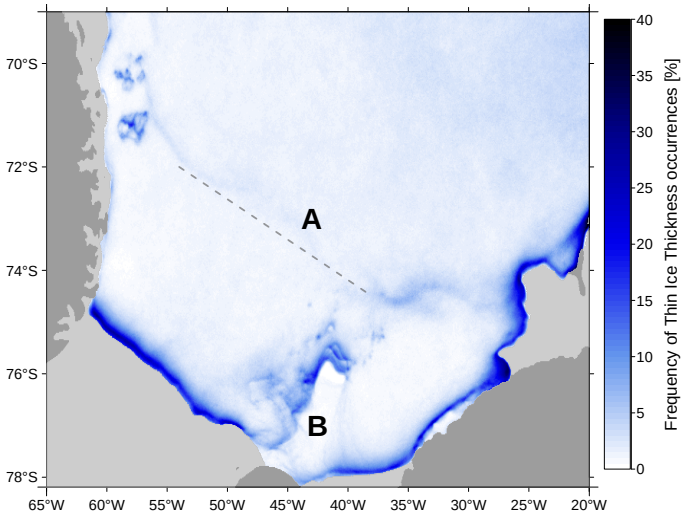

Figure 4. Frequency distribution of thin-ice occurrences in % for the years 2002 to 2014. Shown is the amount of days with thin-ice signal relative to the total number of clear-sky days. The added marks A and B correspond to regional features and are further described in the text.

TCD
9, 3959–3993, 2015

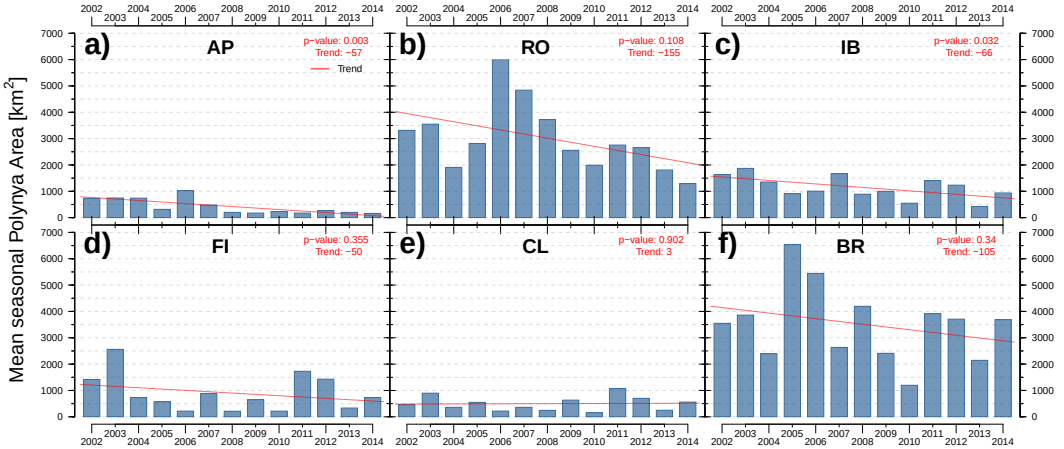

Figure 5. Mean seasonal polynya area [km^2, POLA] for the years from 2002 to 2014 during the winter period from April to September. The red line indicates the multi-year regional trend [km^2 a^{-1}]. *p* value and numeric trend are stated in the top right corner for each sub region.

TCD
9, 3959–3993, 2015

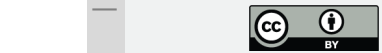

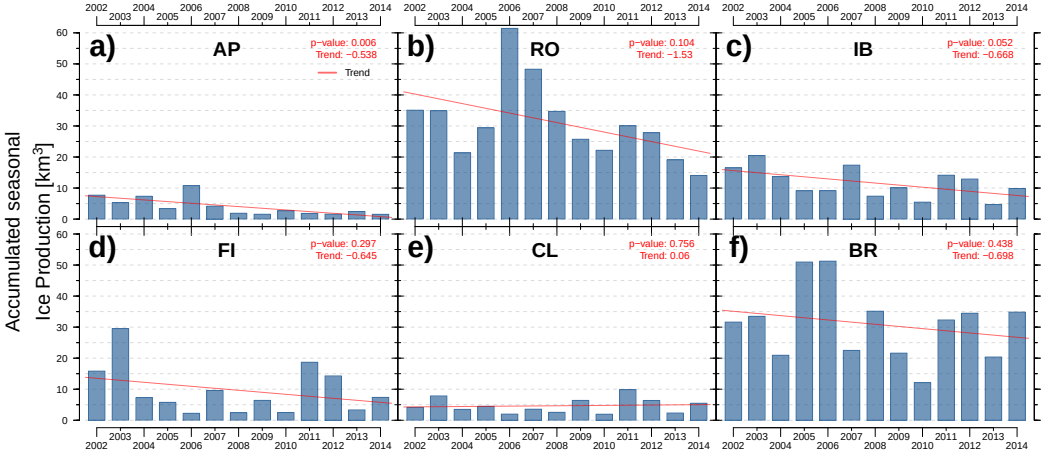

Figure 6. Accumulated seasonal ice production [km^3, IP] for the years from 2002 to 2014 during the winter period from April to September. The red line indicates the multi-year regional trend [$km^3\,a^{-1}$]. *p* value and numeric trend are stated in the top right corner for each sub region.

TCD
9, 3959–3993, 2015

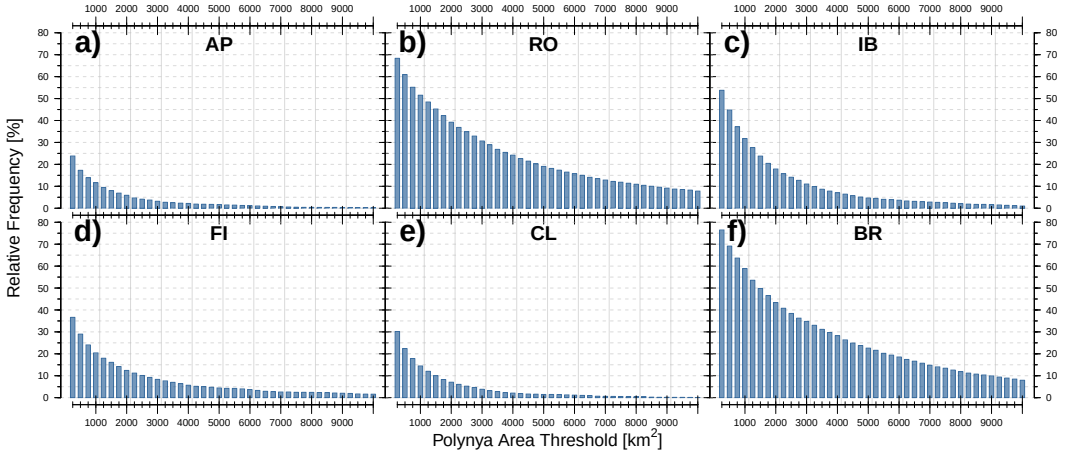

Figure 7. Frequency distribution [%] of days passing the corresponding polynya area threshold [km^2] for the years from 2002 to 2014 during the winter period from April to September. Polynya area thresholds increase by 250 km^2, while estimates below 250 km^2 are not shown.

TCD
9, 3959–3993, 2015

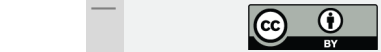

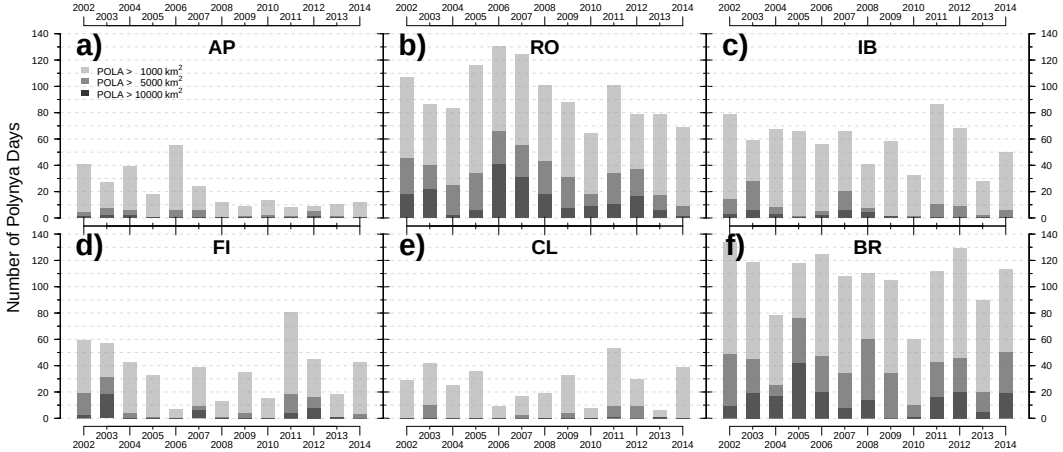

Figure 8. Number of days (polynya days) separated into three polynya area (POLA) classes [km^2] for the years from 2002 to 2014 during the winter period from April to September.

TCD
9, 3959–3993, 2015

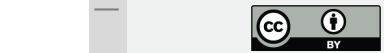

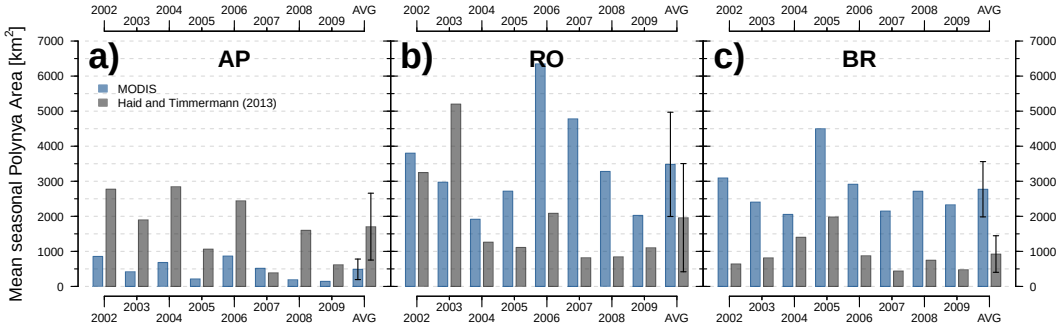

Figure 9. Average seasonal winter-time (May to September) polynya area [km^2, POLA]. Shown is a comparison between our results (blue) and the model results from Haid and Timmermann (2013) (grey) for the years from 2002 to 2009 as well as the multi-year average (AVG) ± one standard deviation (error bars).

TCD
9, 3959–3993, 2015

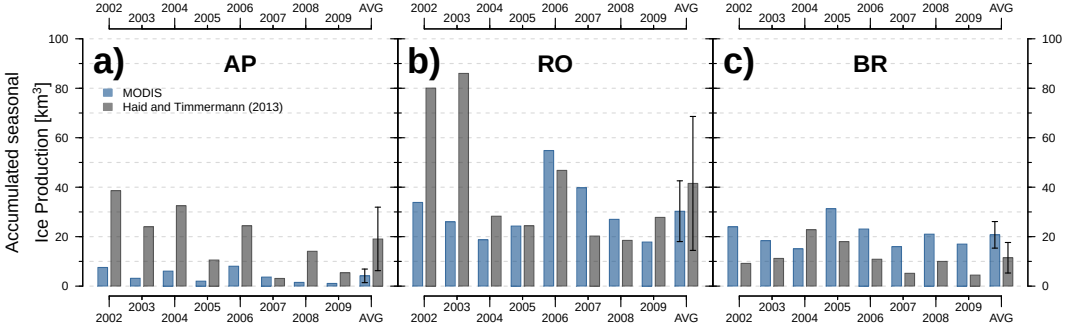

Figure 10. Accumulated ice-production rate [km^3, IP] per winter season (May to September) for the years from 2002 to 2009 in the same setup as Fig. 9.

TCD
9, 3959–3993, 2015

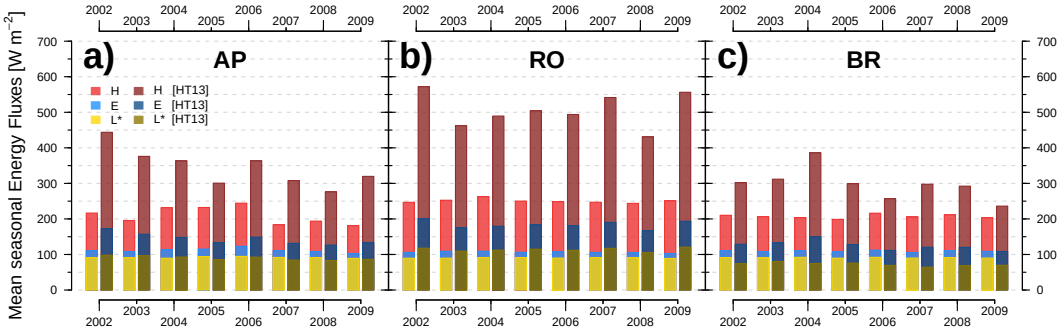

Figure 11. Average winter-time (May to September) energy fluxes of sensible/latent heat (H/E) and net long-wave radiation (L^*) for the years 2002 to 2009 in W m^{-2}. The corresponding model results from Haid and Timmermann (2013) are shown in darker color tones.

TCD
9, 3959–3993, 2015